Monthly Notices of the ROYAL ASTRONOMICAL SOCIETY

MNRAS **464,** 4721–4735 (2017) doi:10.1093/mnras/stw2643
Advance Access publication 2016 October 14

A spectroscopic survey of Herbig Ae/Be stars with X-Shooter – II. Accretion diagnostic lines★

J. R. Fairlamb,[1]† R. D. Oudmaijer,[1]† I. Mendigutia,[1] J. D. Ilee[2] and M. E. van den Ancker[3]

[1]*School of Physics and Astronomy, EC Stoner Building, University of Leeds, Leeds LS2 9JT, UK*
[2] *Institute of Astronomy, Madingley Road, Cambridge CB3 0HA, UK*
[3]*European Southern Observatory (ESO), Karl-Schwarzschild -Str. 2, D-85748 Garching, Germany*

Accepted 2016 October 12. Received 2016 October 10; in original form 2015 October 2

ABSTRACT

The Herbig Ae/Be stars (HAeBes) allow an exploration of the properties of pre-main-sequence(PMS) stars above the low-mass range ($<2\,M_{\odot}$) and those bordering the high-mass range ($>8\,M_{\odot}$). This paper is the second in a series exploring accretion in 91 HAeBes with Very Large Telescope/X-shooter spectra. Equivalent width measurements are carried out on 32 different lines, spanning the UV (ultraviolet) to NIR (near infrared), in order to obtain their line luminosities. The line luminosities were compared to accretion luminosities that were determined directly from measurements of a UV excess. When detected, emission lines always demonstrate a correlation with the accretion luminosity, regardless of detection frequency. The average relationship between accretion luminosity and line luminosity is found to be $L_{\rm acc} \propto L_{\rm line}{}^{1.16\pm0.15}$. This is in agreement with the findings in Classical T Tauri stars, although the HAeBe relationship is generally steeper, particularly towards the Herbig Be mass range. Since all observed lines display a correlation with the accretion luminosity, all of them can be used as accretion tracers. This has increased the number of accretion diagnostic lines in HAeBes 10-fold. However, questions still remain on the physical origin of each line, which may not be due to accretion.

Key words: accretion, accretion discs – techniques: spectroscopic – stars: early-type – stars: formation – stars: pre-main sequence – stars: variables: T Tauri, Herbig Ae/Be.

1 INTRODUCTION

Herbig Ae/Be stars, HAeBes, bridge an important mass range between high- and low-mass stars; namely the intermediate masses of 2–8 $M_{\odot}$. The HAeBes are pre-main-sequence (PMS) stars that display properties such as an infrared excess due to a circumstellar disc (van den Ancker et al. 2000; Meeus et al. 2001), and complex spectral line profiles (Herbig 1960; Finkenzeller & Mundt 1984; Hamann & Persson 1992b); akin to their solar-mass counterparts, the classical T Tauri stars, CTTs (see Bertout 1989, for a review). The HAeBes serve as excellent observational targets that can further our understanding of star formation, as they are readily observable at optical wavelengths unlike the massive young stellar objects, MYSOs that are still heavily embedded in their natal clouds (Mottram et al. 2011).

Theoretical models have long suggested that CTTs accrete via magnetospheric accretion, MA (Ghosh & Lamb 1979; Uchida & Shibata 1985; Koenigl 1991; Shu et al. 1994; Calvet & Gullbring 1998). In this scenario, the circumstellar disc is truncated at a given radius from the star by the stellar magnetic field. The magnetic field lines can then funnel disc material on to the star, at approximately free-fall velocities, via an accretion column. This infalling material shocks the photosphere and gives rise to hotspots on the stellar surface. The result is an excess of ultraviolet (UV) energy that is detectable in addition to the regular photospheric emission. This phenomenon has been observed in numerous CTTs to date (Calvet & Gullbring 1998; Gullbring et al. 1998, 2000; Ingleby et al. 2013), and has been shown to be present in HAeBes (Garrison 1978; Muzerolle et al. 2004; Donehew & Brittain 2011; Mendigutía et al. 2011, 2013; Fairlamb et al. 2015). Provided the stellar parameters are known, the accretion luminosity can be straightforwardly converted into a mass accretion rate, $\dot{M}_{\rm acc}$, one of the key astrophysical parameters in star formation.

It has also been shown that the accretion luminosity ($L_{\rm acc}$) in CTTs, derived from a UV excess or line veiling, is correlated with the luminosity of emission lines ($L_{\rm line}$). This appears to hold true for a large number of lines, such as Brγ, Hα, [O I]$_{\lambda6300}$, and the Ca II

★ Based on observations using the ESO Very Large Telescope, at Cerro Paranal, under the observing program 084.C-0952A

† E-mail: john.fairlamb@gmail.com (JRF); r.d.oudmaijer@leeds.ac.uk (RDO)

IR-triplet (Muzerolle, Hartmann & Calvet 1998; Calvet et al. 2004; Dahm 2008; Herczeg & Hillenbrand 2008; Rigliaco et al. 2012; Alcalá et al. 2014). To date, the luminosity relationships for CTTs have largely been shown to hold for HAeBes too, with only minor changes in intercept and gradient (Mendigutía et al. 2011, 2013). This means that emission lines can be used as powerful accretion diagnostics and provide a method of inferring $\dot{M}_{\rm acc}$ for stars where direct methods of measurement are difficult or impossible e.g. the UV excess is often used to measure $\dot{M}_{\rm acc}$ directly, but UV observations are more difficult to obtain and interpret than simple emission lines; emission lines are also available at a variety of different wavelengths making them a preferred choice over UV observations in highly extinct targets. Therefore, by establishing correlations between the accretion luminosity and line luminosity for a large series of lines, possibilities to infer accretion rates when using data sets with a limited wavelength range are opened.

Changes in the accretion mechanism are suspected to be taking place towards the early-Be stars, as evidenced by spectropolarimetric observations (Vink et al. 2002, 2005). It was also thought that the $L_{\rm acc}$ and $L_{\rm line}$ relationship was breaking down towards HBes by Donehew & Brittain (2011). However, the observed change in the relationship can be explained by the adopted MA model that was for a single cool HAe star. In fact, the observed trends between $L_{\rm acc}$ and $L_{\rm line}$ have been explained by Mendigutía et al. (2015) to be a consequence of the luminosity of the star. Therefore, many observed relationships may not actually be directly due to accretion. However, any observed relationships can still be used to infer an accretion rate, meaning that they remain a valuable tool in this field. Therefore, a large-scale investigation into these relationships for HAeBes is required.

In our previous paper in this series (Fairlamb et al. 2015, hereafter Paper I), we used spectroscopic data from X-Shooter, covering the UV, optical and near-infrared (NIR) wavelengths, to determine the stellar parameters of a large sample of 91 HAeBe stars. Out of this sample, it was possible to determine the UV excess, and thereby the accretion luminosity and mass accretion rates, for 62 of them. The large wavelength range of the data allows for the detection and measurement of many emission lines; observed simultaneously with the UV excess. The large sample is therefore ideal to revisit the hitherto published line luminosities and accretion luminosity relationships, along with an investigation into new accretion diagnostics.

The overall aim of this paper is to provide the measurement of numerous spectral lines across the entire sample of 91 HAeBes. The strengths of the lines are investigated, along with determinations of line luminosities based on previous stellar properties and photometry. These are compared against the accretion rates determined in Paper I in order to provide a critical assessment of accretion luminosity versus line luminosity relationships in HAeBes.

This paper is organized as follows. Section 2 provides details on the sample, data reduction and techniques of emission line measurements and line luminosity calculations. Section 3 presents the measurements of the lines, calculated line luminosities and the resulting correlations with the accretion luminosity. Analysis of these relationships and the presentation of new accretion diagnostics are provided in this section too. Finally, Section 4 provides a summary of the results and the concluding remarks.

2 SAMPLE, OBSERVATIONS, DATA REDUCTION, AND MEASUREMENTS

The sample, observations and basic data reduction processes are detailed in Paper I. We give a brief summary of these here, while we discuss the correction for telluric absorption lines and go into details on the measurement of line strengths. The stars were selected from the catalogues of HAeBe stars published by Thé, de Winter & Perez (1994) and Vieira et al. (2003). The main criterion to be included the sample was their observability in the Southern hemisphere during the (southern) summer semester. In total, the sample contains 91 stars, of which 37 have a mass greater than 3 $M_{\odot}$, which we choose to classify as the Herbig Be stars. The remaining stars are all HAes, with perhaps a few intermediate-mass CTTs that border the mass boundary.

The observations were carried out with X-Shooter mounted on the ESO's VLT, UT3, Paranal, Chile in the 2009–2010 season (Vernet et al. 2011). The instrument provides complete coverage from 0.3 to 2.4 μm over three separate arms; the arms are split into the following: the UVB arm, 3000–5600 Å; the VIS arm, 5500–10 200 Å and the NIR arm, 10 200–24 800 Å. The observations were taken with the smallest possible slit widths resulting in a spectral resolution of 10 000–18 000.

The integration times were such that signal-to-noise ratios (SNRs) of 100–200 were typical. The bias subtraction, flat fielding and wavelength calibration were all performed using the ESO pipeline reduction (Modigliani et al. 2010). When available, data were taken from the recent phase III release with pipeline version 2.3.12. For the small number where this was not the case, the reduced data from Paper I (pipeline version 0.9.7) are taken. In general, the quality of the reduced data in both cases is similar, except in the NIR arm where the SNR is better in the phase III data.

The spectra were not flux calibrated as a matter of course, and instead we use published photometry of all our sources when computing the final line luminosities (see Paper I for details of photometry sources). Since the typical errors in the flux determination from spectrophotometric data amount to around 20 per cent, this choice is warranted for objects that vary less than 20 per cent (or roughly 0.2 mag). It has been shown in PMS stars that the variability amplitude decreases with increasing wavelength e.g. for a change in the *V*-band of 0.4 mag changes in the *K*-band are generally less than 0.2 mag (Eiroa et al. 2001, 2002). Spot-checks on our targets indicate that the variability is indeed at most of this order on average, validating the choice of using existing photometry. Due to the large sample used any objects with large variability changes, which could produce anomalous results, are likely to be identified or their effects diluted by the sheer number of other targets used.

2.1 Correction for telluric absorption lines

Before measurements of the lines are undertaken, telluric absorption features in the spectra must be removed. This is particularly necessary for the majority of the observable emission lines in the NIR arm, but also for a few cases in the VIS arm covering the optical.

A telluric standard star can be used for such a correction, but these stars contain their own spectral features that also need to be corrected for. Since many of the lines observed are hydrogen recombination lines that are commonly seen in absorption in telluric standard stars, correction is instead performed using the ESO MOLECFIT[1] telluric removal tool (Kausch et al. 2015; Smette et al. 2015). There are a few additional issues that contributed to rejecting the telluric standards and using MOLECFIT instead: airmass could differ by large amounts (mostly uncommon) and short exposure times

[1] http://www.eso.org/sci/software/pipelines/skytools/molecfit

of the tellurics (on average the SNR was half that of the targets). MOLECFIT provides an atmospheric transmission spectrum using a radiative transfer code based on a combination of the observatory conditions at that time and the features observed in the target spectra. Removal of the lines using both MOLECFIT and telluric standards was compared and it was found that using MOLECFIT yielded better quality spectra over using the telluric standards; the SNR of the latter contributes to a poorer reduction.

Therefore, MOLECFIT correction is performed on all spectral orders in each arm that contains telluric line features, and will be used for the remainder of this paper (see also Ilee et al. 2014, where MOLECFIT is used in the same way to study the CO overtone emission at 2.3μm).

2.2 Measuring emission line strengths

After telluric corrections, line strengths are recorded by measuring the equivalent widths, EW, of the lines after normalizing the spectra of each star to the continuum level. These direct measurements of the EW will be referred to as EW_{obs}. In order to obtain the true line strengths of the emission lines EW_{obs} needs to be corrected for both the underlying photospheric absorption, EW_{int}, and the presence of any excess continuum emission, which would dilute the underlying absorption.

The photospheric absorption depends upon the temperature, surface gravity and metallicity of the stars. The temperature and surface gravity of each star were determined in Paper I and are used to select an appropriate spectral model atmosphere, from which the absorption line strengths are measured. In this work, the Munari set of Kurucz–Castelli models, KC-models, are used for lines with $\lambda < 10050$ Å, due to their 1 Å sampling (Munari et al. 2005); a metallicity of $[M/H] = 0$ is adopted. For longer wavelengths, additional models are required, the older KC-models are used here computed by Kurucz (1993) and Castelli & Kurucz (2004). For consistency, the region of measurement used for EW_{obs} is also used for measuring EW_{int}. Fig. 1 provides an example of the intrinsic absorption strength as a function of temperature for some of the lines (log(g) is fixed in this example).

The net emission, which is stronger than the straightforward measurement of EW_{obs} would imply, can now be corrected for the intrinsic absorption. The corrected equivalent width, EW_{cor}, is calculated as follows:

$$EW_{cor} = EW_{obs} - 10^{-0.4\Delta m_{\lambda}} EW_{int} \quad (1)$$

where Δm_{λ} is the strength of the continuum excess at the wavelength in question, measured in magnitudes. It is the difference between the observed, dereddened magnitude and the intrinsic magnitude of a star of the same spectral type.

Fig. 2 demonstrates the importance of correcting for intrinsic absorption. In the figure, it can be seen that UX Ori definitely has emission present. However, when measuring EW_{obs} a positive value is obtained i.e. an absorption line. Correcting for EW_{int} makes EW_{cor} negative, and therefore in emission. The benefit of this approach is that the result encompasses all of the true emission.

At NIR wavelengths excess emission is also present, due to thermal emission from circumstellar dust heated by the central star. That is there is a non-zero Δm_{λ} component, for the majority of stars, because of the IR excess. In order to obtain Δm_{λ}, the intrinsic magnitude is first obtained by scaling a KC-model of the same stellar parameters to match the dereddened visible photometry of the star and measuring the flux from the model at the wavelength in question (the compiled photometry is listed in Paper I). To avoid

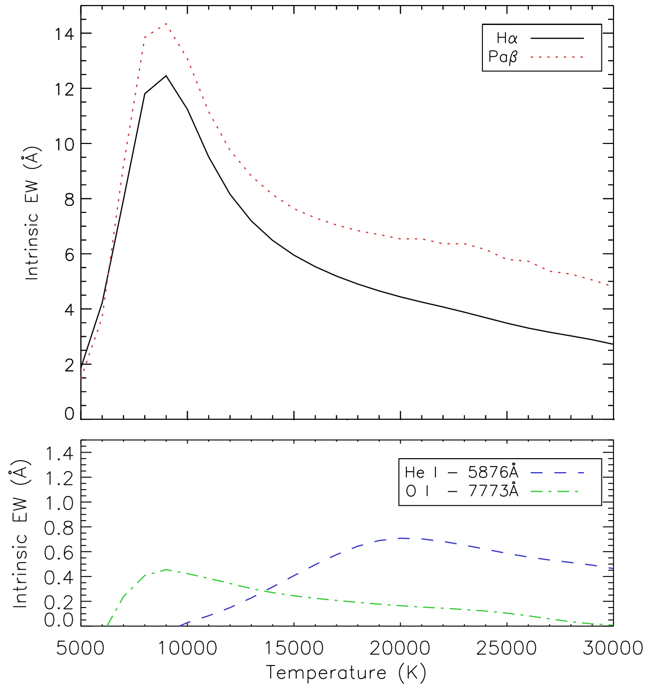

Figure 1. The two panels above show how EW_{int} varies as a function of temperature. More importantly, it demonstrates that the variation is significantly different between different elements e.g. Hydrogen absorption peaks at ∼9000 K, while Helium absorption peaks at ∼20 000 K.

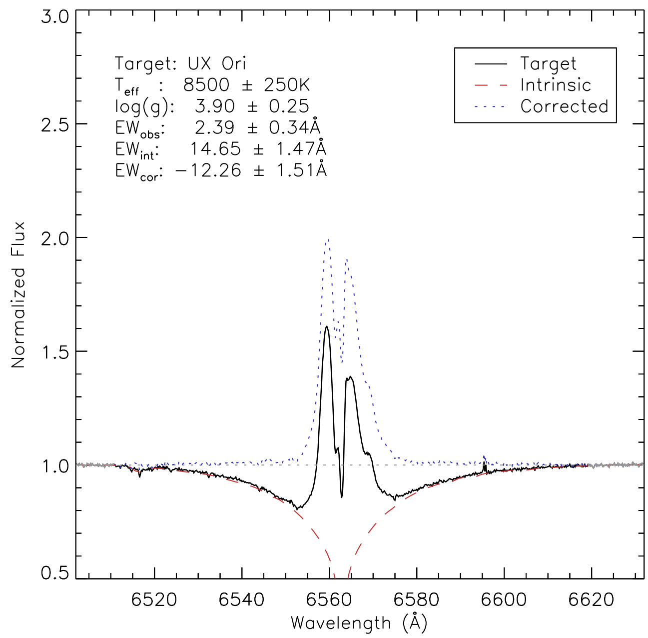

Figure 2. The Hα line for UX Ori is displayed here; the original spectra is shown in black. Also plotted here are: the predicted intrinsic spectra, red-dashed; the corrected spectra, blue-dotted; the continuum level, grey-dashed; and finally the left and right continuum regions that are used for normalizing the lines, solid-grey. The left-hand legend details the properties of UX Ori. The figure demonstrates that despite clear emission a positive EW_{obs} can be measured. Therefore, it is also important to assess EW_{int} when examining the strength of lines.

underestimating the continuum flux, which can be affected by the underlying absorption in the model, an interpolation of the continuum regions either side of the line is used to derive the continuum flux. This is then converted into a magnitude to give the expected intrinsic magnitude (since this is at an arbitrary wavelength no convolutions with pass-bands are involved). Next, this must be compared against the observed dereddened magnitude. This uses the *JHK* photometric data from 2MASS (Cutri et al. 2003; Skrutskie et al. 2006). The photometry is dereddened and converted into a flux using the A_V values determined in Paper I, and then an interpolation is made between the photometric points either side of the wavelength in question (and converted back into a magnitude). With both the observed and expected intrinsic magnitudes obtained, Δm_λ is found via the difference; $\mathrm{EW_{cor}}$ can now be calculated.

2.3 Error budget

A consideration of errors needs to be made in all the above steps. Let us first start with the line measurement itself. Since $\mathrm{EW_{obs}}$ is a numerical calculation over a wavelength region, the error will be the extent of this region, $\Delta\lambda$ divided by the SNR of the continuum: $\sigma_{\mathrm{EWobs}} = \Delta\lambda/\mathrm{SNR}$. The error on $\mathrm{EW_{int}}$ is also complicated by stellar parameters, metallicity and the adopted set of models. For this reason a generous error of 10 per cent is adopted for all $\mathrm{EW_{int}}$ measured from the Munari set of KC-models; an error of 20 per cent is adopted for the NIR lines measured from the lower resolution models. Errors in Δm_λ are low, due to the quality of the *JHK* photometry, and the relatively low errors in the stellar parameters. Since the EW errors dominate over Δm_λ only the $\mathrm{EW_{obs}}$ and $\mathrm{EW_{int}}$ errors are considered in $\mathrm{EW_{cor}}$. With $\mathrm{EW_{cor}}$ established, a line flux, F_{line}, can now be calculated by $F_{\mathrm{line}} = \mathrm{EW_{cor}} \times F_\lambda$, where F_λ is the continuum flux corresponding to the central wavelength of the line. For all lines with line centres $<1\ \mu$m, F_λ is calculated from a KC-model in the same way the intrinsic magnitude was calculated earlier (but omitting the final magnitude conversion). For the lines with line centres $>1\ \mu$m, an interpolation of the dereddened *JHK* photometry is performed in the same manner as was done for obtaining the IR excess magnitude earlier, except a further step is required of converting this into a flux.

Expanding upon this, a line luminosity, L_{line}, is also calculated by $L_{\mathrm{line}} = 4\pi D^2\, F_{\mathrm{line}}$, where D is the distance to star (the values used are complied in Paper I). The L_{line} value takes into account both errors on the distance and the stellar parameters used to calculate F_{line}. A complete list of errors on L_{line} are included in the online version of Table 1.

3 RESULTS

In total, $\mathrm{EW_{obs}}$, $\mathrm{EW_{int}}$, $\mathrm{EW_{cor}}$ and the corresponding line luminosities are calculated for a set of 32 different lines. The lines were selected based on being observed previously in the literature, or by having a high detection rate throughout the sample; preferably both. These lines span the full wavelength range covered. To put the number of lines into perspective, we note that lines previously identified in the literature as accretion diagnostics for HAeBes stars are limited to Hα, [O I]6300 and Brγ (Donehew & Brittain 2011; Mendigutía et al. 2011); hence the number of lines investigated in this manner has increased 10-fold.

The EW, F_{line}, and L_{line} data for the Hα line are provided in Table 1. The table contains this information for all of the observed targets. A further 31 lines have been measured and are available online.

The following sections investigate the empirical relationship between the line luminosities and the accretion luminosities, along with a comparison against CTTs.

3.1 Accretion luminosity–line luminosity relationships

In Fig. 3, the relationship between the accretion luminosity L_{acc}, derived for 62 stars using the UV excess, is shown plotted against the luminosity of six different emission lines. The selected lines are He I$_{\lambda5876}$, Hα, O I$_{\lambda7773}$, He I$_{\lambda10830}$, Paβ, and Brγ as they cover a large wavelength range and a few different elemental species. Correlations for other lines are available in the online version of this paper.

The line luminosity–accretion luminosity relationship can be approximated by a power law, and has been in numerous works on CTTs and HAeBes (Muzerolle et al. 1998; Calvet et al. 2004; Dahm 2008; Herczeg & Hillenbrand 2008; Mendigutía et al. 2011; Rigliaco et al. 2012), where

$$\log\left(\frac{L_{\mathrm{acc}}}{\mathrm{L}_\odot}\right) = A + B \times \log\left(\frac{L_{\mathrm{line}}}{\mathrm{L}_\odot}\right) \quad (2)$$

where A and B are constants describing the intercept and slope, respectively. Such a relationship is obtained across all lines for the Herbig Ae/Be stars; the slopes and intercepts are presented in Table 2. The best fits were calculated using the IDL *mpfitexy* package that factors in errors in both the x- and y-axis. Fig. A1, in the appendix, displays the correlations for all lines observed; Table 2 provides details of the correlations. Where possible, the findings of Alcalá et al. (2014) on a set of CTTs are shown in these figures for comparison. The same relationship between the line and accretion luminosities observed for CTTs, and reported previously in HAeBes, extends to other lines as well. Indeed, this trend is essentially observed for *all* lines. The strong correlation between line luminosity and accretion luminosity is the reason why emission lines are a useful tool for easily determining accretion luminosities (and in turn determining the mass accretion rate).

A comparison with previous determinations of the slope and intercept derived in the literature for Herbig Ae/Be stars is made here. Specifically the Hα, [O I]$_{\lambda6300}$ and Brγ relationships from Mendigutía et al. (2011) are assessed. It is found that the relationships obtained here agree with previous work; they lie within the error bars of each other. The main difference here is that the errors, particularly on the intercept, are reduced here. This is presumably due to the increased sample size and simultaneity of the observations of the UV excess and lines.

The relationship for Brγ in this paper agrees well with Mendigutía et al. (2011). Both these relationships do not agree with the breakdown in Brγ relationship implied by Donehew & Brittain (2011). This can be attributed to the MA models used in the latter being associated with a relatively low-mass HAeBe star, producing lower accretion luminosities than expected; their model was based on UX Ori from Muzerolle et al. (2004), while this work focuses on multiple models from Mendigutía et al. (2011) and Paper I. Therefore, we can say that there remains a L_{acc}–L_{line} relationship for HAeBes.

3.2 Comparison with T Tauri stars

The data on CTTs from Alcalá et al. (2014) for the lines in common with this study are also included for comparison, along with their best fit in Fig. A1. Overall, the plots appear to show a qualitative agreement in trends between the HAeBes and the CTTs, where L_{acc}

Table 1. This table provides the EW measurements for the Hα line in all objects. A full version of this table containing all 32 lines is available online. It is worth noting that the Δm_λ column contains no values for this particular line as no correction for an excess is required; an IR-excess correction is required for lines >1 μm. In column 6, containing the line flux, the 'E$-x$' factor denotes $\times\ 10^x$.

Name	Details of the Hα line					
	EW_{obs} (Å)	EW_{int} (Å)	Δm_λ (mag)	EW_{cor} (Å)	F_{line} (Wm^{-2} Å^{-1})	log(L_{line}) [$L_\odot$]
UX Ori	2.39 ± 0.34	14.65 ± 1.47	–	−12.26 ± 1.51	3.27 (± 0.40) E -15	−1.43 ± 0.10
PDS 174	−54.19 ± 1.34	6.46 ± 0.65	–	−60.65 ± 1.49	2.33 (± 0.06) E -14	−0.03 ± 0.09
V1012 Ori	4.74 ± 0.55	16.36 ± 1.64	–	−11.62 ± 1.73	1.42 (± 0.21) E -15	−2.06 ± 0.11
HD 34282	4.18 ± 0.40	16.23 ± 1.62	–	−12.05 ± 1.67	3.03 (± 0.42) E -15	−1.90 ± 0.11
HD 287823	10.18 ± 0.50	15.58 ± 1.56	–	−5.40 ± 1.64	1.64 (± 0.50) E -15	−2.23 ± 0.16
HD 287841	8.36 ± 0.43	13.22 ± 1.32	–	−4.86 ± 1.39	9.64 (± 2.75) E -16	−2.46 ± 0.15
HD 290409	0.35 ± 0.55	15.00 ± 1.50	–	−14.65 ± 1.60	3.18 (± 0.35) E -15	−1.58 ± 0.10
HD 35929	1.54 ± 0.69	8.69 ± 0.87	–	−7.15 ± 1.11	1.09 (± 0.17) E -14	−1.35 ± 0.11
HD 290500	−1.46 ± 0.25	13.14 ± 1.31	–	−14.60 ± 1.33	1.26 (± 0.11) E -15	−1.04 ± 0.10
HD 244314	−14.04 ± 0.61	15.54 ± 1.55	–	−29.58 ± 1.67	6.91 (± 0.39) E -15	−1.38 ± 0.09
HK Ori	−61.86 ± 0.72	15.79 ± 1.58	–	−77.65 ± 1.74	1.51 (± 0.03) E -14	−1.04 ± 0.09
HD 244604	2.32 ± 0.51	14.79 ± 1.48	–	−12.47 ± 1.57	5.72 (± 0.72) E -15	−1.46 ± 0.10
UY Ori	4.98 ± 0.26	15.28 ± 1.53	–	−10.30 ± 1.55	4.81 (± 0.72) E -16	−1.80 ± 0.11
HD 245185	−13.56 ± 0.50	14.48 ± 1.45	–	−28.04 ± 1.53	6.54 (± 0.36) E -15	−1.26 ± 0.09
T Ori	−4.15 ± 0.43	13.07 ± 1.31	–	−17.22 ± 1.38	1.04 (± 0.08) E -14	−0.74 ± 0.09
V380 Ori	−81.88 ± 0.48	13.61 ± 1.36	–	−95.49 ± 1.44	9.74 (± 0.15) E -14	−0.48 ± 0.09
HD 37258	−0.33 ± 0.39	15.00 ± 1.50	–	−15.33 ± 1.55	4.88 (± 0.49) E -15	−1.56 ± 0.10
HD 290770	−24.08 ± 0.35	12.98 ± 1.30	–	−37.06 ± 1.35	1.57 (± 0.06) E -14	−1.02 ± 0.09
BF Ori	−0.02 ± 0.46	14.70 ± 1.47	–	−14.72 ± 1.54	5.35 (± 0.56) E -15	−1.36 ± 0.10
HD 37357	4.76 ± 0.41	14.64 ± 1.46	–	−9.88 ± 1.52	6.32 (± 0.97) E -15	−1.63 ± 0.11
HD 290764	−2.38 ± 0.43	13.31 ± 1.33	–	−15.69 ± 1.40	5.03 (± 0.45) E -15	−1.46 ± 0.10
HD 37411	−1.07 ± 0.47	15.55 ± 1.56	–	−16.62 ± 1.63	5.29 (± 0.52) E -15	−1.67 ± 0.10
V599 Ori	1.69 ± 0.57	13.35 ± 1.34	–	−11.66 ± 1.46	6.48 (± 0.81) E -15	−1.28 ± 0.10
V350 Ori	3.09 ± 0.33	15.66 ± 1.57	–	−12.57 ± 1.60	2.52 (± 0.32) E -15	−1.69 ± 0.10
HD 250550	−48.83 ± 0.39	10.03 ± 1.00	–	−58.86 ± 1.07	2.01 (± 0.04) E -14	−0.22 ± 0.09
V791 Mon	−88.08 ± 0.25	7.94 ± 0.79	–	−96.02 ± 0.83	4.22 (± 0.04) E -14	−0.26 ± 0.09
PDS 124	−13.83 ± 1.37	14.13 ± 1.41	–	−27.96 ± 1.97	2.02 (± 0.14) E -15	−1.30 ± 0.09
LkHa 339	−5.39 ± 1.37	12.98 ± 1.30	–	−18.37 ± 1.89	4.24 (± 0.44) E -15	−1.33 ± 0.10
VY Mon	−17.81 ± 1.76	8.45 ± 0.84	–	−26.26 ± 1.95	6.94 (± 0.52) E -14	−0.38 ± 0.09
R Mon	−114.51 ± 1.76	9.35 ± 0.93	–	−123.86 ± 1.99	4.22 (± 0.07) E -14	−0.07 ± 0.09
V590 Mon	−60.10 ± 0.52	9.63 ± 0.96	–	−69.73 ± 1.09	3.46 (± 0.05) E -15	−0.49 ± 0.09
PDS 24	−25.47 ± 1.79	12.98 ± 1.30	–	−38.45 ± 2.21	1.17 (± 0.07) E -15	−1.00 ± 0.09
PDS 130	−31.17 ± 0.70	11.41 ± 1.14	–	−42.58 ± 1.34	2.75 (± 0.09) E -15	−0.58 ± 0.09
PDS 229N	7.41 ± 0.82	9.63 ± 0.96	–	−2.22 ± 1.26	1.72 (± 0.97) E -16	−1.99 ± 0.26
GU CMa	−14.86 ± 0.48	4.75 ± 0.47	–	−19.61 ± 0.67	1.61 (± 0.06) E -13	0.15 ± 0.09
HT CMa	−20.94 ± 0.35	11.87 ± 1.19	–	−32.81 ± 1.24	1.75 (± 0.07) E -15	−0.84 ± 0.09
Z CMa	−63.55 ± 0.99	9.97 ± 1.00	–	−73.52 ± 1.41	7.72 (± 0.15) E -13	1.43 ± 0.09
HU CMa	−52.00 ± 0.40	9.09 ± 0.91	–	−61.09 ± 0.99	6.64 (± 0.11) E -15	−0.50 ± 0.09
HD 53367	−7.62 ± 0.52	4.02 ± 0.40	–	−11.64 ± 0.66	2.15 (± 0.12) E -13	−0.11 ± 0.09
PDS 241	−8.36 ± 0.29	4.21 ± 0.42	–	−12.57 ± 0.51	4.32 (± 0.17) E -15	0.06 ± 0.09
NX Pup	−37.01 ± 0.45	8.74 ± 0.87	–	−45.75 ± 0.98	1.75 (± 0.04) E -14	−1.04 ± 0.09
PDS 27	−73.20 ± 0.73	4.40 ± 0.44	–	−77.60 ± 0.85	1.08 (± 0.01) E -13	1.53 ± 0.09
PDS 133	−103.11 ± 3.91	7.84 ± 0.78	–	−110.95 ± 3.99	4.99 (± 0.18) E -15	−0.01 ± 0.09
HD 59319	5.86 ± 6.14	7.13 ± 0.71	–	−1.27 ± 6.18	< 1.19 E -15	< −1.26
PDS 134	−12.22 ± 0.41	5.98 ± 0.60	–	−18.20 ± 0.73	1.58 (± 0.06) E -15	0.20 ± 0.09
HD 68695	0.48 ± 0.48	16.51 ± 1.65	–	−16.03 ± 1.72	4.18 (± 0.45) E -15	−1.81 ± 0.10
HD 72106	8.78 ± 0.63	14.60 ± 1.46	–	−5.82 ± 1.59	4.77 (± 1.30) E -15	−1.69 ± 0.15
TYC 8581-2002-1	11.05 ± 0.42	13.61 ± 1.36	–	−2.56 ± 1.42	3.50 (± 1.95) E -16	−2.05 ± 0.26
PDS 33	−3.10 ± 0.48	15.83 ± 1.58	–	−18.93 ± 1.65	7.90 (± 0.69) E -16	−1.67 ± 0.09
HD 76534	−11.00 ± 0.34	5.84 ± 0.58	–	−16.84 ± 0.67	3.63 (± 0.15) E -14	−0.44 ± 0.09
PDS 281	4.30 ± 0.49	5.42 ± 0.54	–	−1.12 ± 0.73	3.81 (± 2.48) E -15	−0.98 ± 0.30
PDS 286	−26.84 ± 0.42	3.93 ± 0.39	–	−30.77 ± 0.57	2.75 (± 0.05) E -13	0.37 ± 0.09
PDS 297	7.42 ± 0.41	11.36 ± 1.14	–	−3.94 ± 1.21	2.80 (± 0.86) E -16	−1.73 ± 0.16
HD 85567	−50.25 ± 0.47	6.76 ± 0.68	–	−57.01 ± 0.83	1.09 (± 0.02) E -13	0.45 ± 0.09
HD 87403	6.79 ± 0.63	9.76 ± 0.98	–	−2.97 ± 1.17	1.27 (± 0.50) E -15	−0.89 ± 0.19
PDS 37	−119.89 ± 0.47	3.87 ± 0.39	–	−123.76 ± 0.61	2.53 (± 0.01) E -13	2.17 ± 0.09
HS 305298	0.01 ± 0.41	3.25 ± 0.32	–	−3.24 ± 0.52	9.93 (± 1.59) E -16	−0.45 ± 0.11
HD 94509	−16.84 ± 0.53	6.33 ± 0.63	–	−23.17 ± 0.82	1.09 (± 0.04) E -14	0.82 ± 0.09

Table 1 – *continued*

Name	EW_{obs} (Å)	EW_{int} (Å)	Δm_λ (mag)	EW_{cor} (Å)	F_{line} (Wm^{-2} Å^{-1})	$\log(L_{line})$ [$L_\odot$]
			Details of the XXXXXX line			
HD 95881	−12.53 ± 0.39	9.35 ± 0.94	–	−21.88 ± 1.02	2.60 (± 0.12) E -14	0.13 ± 0.09
HD 96042	3.20 ± 0.80	3.95 ± 0.39	–	−0.75 ± 0.89	< 1.27 E -15	< −0.90
HD 97048	−24.43 ± 0.34	13.54 ± 1.35	–	−37.97 ± 1.39	8.06 (± 0.30) E -14	−1.13 ± 0.09
HD 98922	−14.64 ± 0.44	10.04 ± 1.00	–	−24.68 ± 1.09	1.16 (± 0.05) E -13	−0.36 ± 0.09
HD 100453	5.27 ± 0.77	10.23 ± 1.02	–	−4.96 ± 1.28	9.50 (± 2.45) E -15	−2.35 ± 0.14
HD 100546	−23.96 ± 0.42	15.50 ± 1.55	–	−39.46 ± 1.61	1.76 (± 0.07) E -13	−1.29 ± 0.09
HD 101412	−0.15 ± 0.69	15.28 ± 1.53	–	−15.43 ± 1.68	8.38 (± 0.91) E -15	−1.62 ± 0.10
PDS 344	−22.23 ± 0.45	7.80 ± 0.78	–	−30.03 ± 0.90	7.69 (± 0.23) E -16	−0.74 ± 0.09
HD 104237	−13.74 ± 0.98	13.75 ± 1.38	–	−27.49 ± 1.69	1.61 (± 0.10) E -13	−1.18 ± 0.09
V1028 Cen	−101.61 ± 0.52	7.01 ± 0.70	–	−108.62 ± 0.87	2.22 (± 0.02) E -14	0.37 ± 0.09
PDS 361S	−3.97 ± 0.45	5.35 ± 0.53	–	−9.32 ± 0.70	8.10 (± 0.60) E -16	−0.31 ± 0.09
HD 114981	−7.60 ± 0.46	5.64 ± 0.56	–	−13.24 ± 0.72	3.37 (± 0.18) E -14	−0.06 ± 0.09
PDS 364	−78.38 ± 0.74	9.63 ± 0.96	–	−88.01 ± 1.21	4.40 (± 0.06) E -15	−0.39 ± 0.09
PDS 69	−69.42 ± 1.30	7.00 ± 0.70	–	−76.42 ± 1.48	8.40 (± 0.16) E -14	0.02 ± 0.09
DG Cir	−47.98 ± 0.83	13.10 ± 1.31	–	−61.08 ± 1.55	6.27 (± 0.16) E -15	−1.00 ± 0.09
HD 132947	10.38 ± 0.33	11.96 ± 1.20	–	−1.58 ± 1.24	9.04 (± 7.12) E -16	−2.04 ± 0.35
HD 135344B	−4.60 ± 0.75	5.66 ± 0.57	–	−10.26 ± 0.94	1.35 (± 0.12) E -14	−2.08 ± 0.10
HD 139614	0.48 ± 0.61	13.26 ± 1.33	–	−12.78 ± 1.46	1.33 (± 0.15) E -14	−2.09 ± 0.10
PDS 144S	−16.12 ± 0.68	13.07 ± 1.31	–	−29.19 ± 1.48	9.49 (± 0.48) E -16	−1.53 ± 0.09
HD 141569	5.13 ± 0.57	15.55 ± 1.56	–	−10.42 ± 1.66	3.36 (± 0.54) E -14	−1.88 ± 0.11
HD 141926	−43.48 ± 0.43	3.40 ± 0.34	–	−46.88 ± 0.55	3.00 (± 0.04) E -13	1.17 ± 0.09
HD 142666	5.14 ± 0.68	11.70 ± 1.17	–	−6.56 ± 1.35	9.17 (± 1.89) E -15	−2.22 ± 0.12
HD 142527	−6.95 ± 0.98	6.18 ± 0.62	–	−13.13 ± 1.16	1.91 (± 0.17) E -14	−1.93 ± 0.10
HD 144432	−0.98 ± 0.68	11.65 ± 1.17	–	−12.63 ± 1.35	1.76 (± 0.19) E -14	−1.85 ± 0.10
HD 144668	−8.41 ± 0.45	14.12 ± 1.41	–	−22.53 ± 1.48	1.40 (± 0.09) E -13	−0.95 ± 0.09
HD 145718	8.34 ± 0.52	14.53 ± 1.45	–	−6.19 ± 1.54	6.86 (± 1.71) E -15	−2.34 ± 0.14
PDS 415N	3.10 ± 1.30	5.04 ± 0.50	–	−1.94 ± 1.39	2.45 (± 1.76) E -16	−3.53 ± 0.32
HD 150193	−5.59 ± 0.57	16.07 ± 1.61	–	−21.66 ± 1.71	6.21 (± 0.49) E -14	−1.55 ± 0.09
AK Sco	−0.82 ± 0.95	5.06 ± 0.51	–	−5.88 ± 1.08	4.81 (± 0.88) E -15	−2.60 ± 0.12
PDS 431	1.27 ± 0.50	10.49 ± 1.05	–	−9.22 ± 1.16	4.41 (± 0.56) E -16	−0.94 ± 0.10
KK Oph	−25.15 ± 0.31	16.36 ± 1.64	–	−41.51 ± 1.67	1.28 (± 0.05) E -14	−1.50 ± 0.09
HD 163296	−3.63 ± 0.36	16.02 ± 1.60	–	−19.65 ± 1.64	7.82 (± 0.65) E -14	−1.60 ± 0.09
MWC 297	−590.00 ± 0.90	4.52 ± 0.45	–	−594.52 ± 1.01	4.68 (± 0.01) E -11	1.63 ± 0.09

is increasing proportionally to $L_{\rm line}$, generally a 1:1 correlation. The placement of the CTTs and HAeBes in the plots often agrees with each where they transition between each other, suggesting similarity between the two groups. An exception is the Ca II triplet where there is an offset, likely due to blending with the Paschen series. The best-fitting relationship to the HAeBes is generally steeper than it is for the extrapolated CTTs best fit, suggesting a possible difference in the origin of the line luminosity. However, this is not true in all cases and the average of all relationships are in agreement with each other. The slope of the $L_{\rm acc}$ versus $L_{\rm line}$ relationship, the B value, is found to have an average of $\bar{B} = 1.16 \pm 0.15$ in the HAeBes, while for the CTTs it is $\bar{B} = 1.08 \pm 0.08$. The values of the best-fitting relationships for the CTTs and the HAeBes are provided in Table 2.

Overall, it appears that the relationship between $L_{\rm acc}$ and $L_{\rm line}$, for all lines, is well correlated in HAeBes. This confirms the predictions of Mendigutía et al. (2015) that the relationship is a mathematical one tied to the luminosity stars rather than the actual strengths of the lines. The slope of the relationships obtained here are slightly enhanced over the set of CTTs analysed by Alcalá et al. (2014). A small level of caution should be noted if using the relationships of the Ca II triplet due to Paschen blending that may be causing the offset observed between HAeBes and CTTs. Another note of caution is advised when using the He I and O I lines, as their complex line profiles suggest various origins – which may or may not be associated with accretion. The complexities of their profiles are likely the cause of the low detection rate of these lines, as multiple absorption and emission components can contribute to the line equivalent width. An exploration of the line profiles will be presented in a future paper by the authors.

3.3 Emission lines as accretion diagnostics

Since all of the emission lines appear to be correlated with the accretion luminosity, it is worth discussing which lines serve as the most sensitive tracers of accretion i.e. most readily detected (and therefore possibly associated directly with accretion). That way the best lines can be prioritized in future observations.

In Table 3, all 32 lines are presented along with details of the number of emission detections. The other columns of the table are split into different categories based on emission detection and UV-excess detection. HAeBe stars that are classed as having an accretion detection are those for which a UV excess was clearly detected in Paper I – 62 stars match this criterion. This includes the seven stars in which an accretion rate could not be determined within the context of MA; it would require an unrealistically high filling factor of shocked material to reproduce their UV excess. The measured ΔD_B of these seven objects is likely associated with accretion due to the overall properties of the stars, although the exact mechanism is not known [an alternative could be boundary layer accretion for

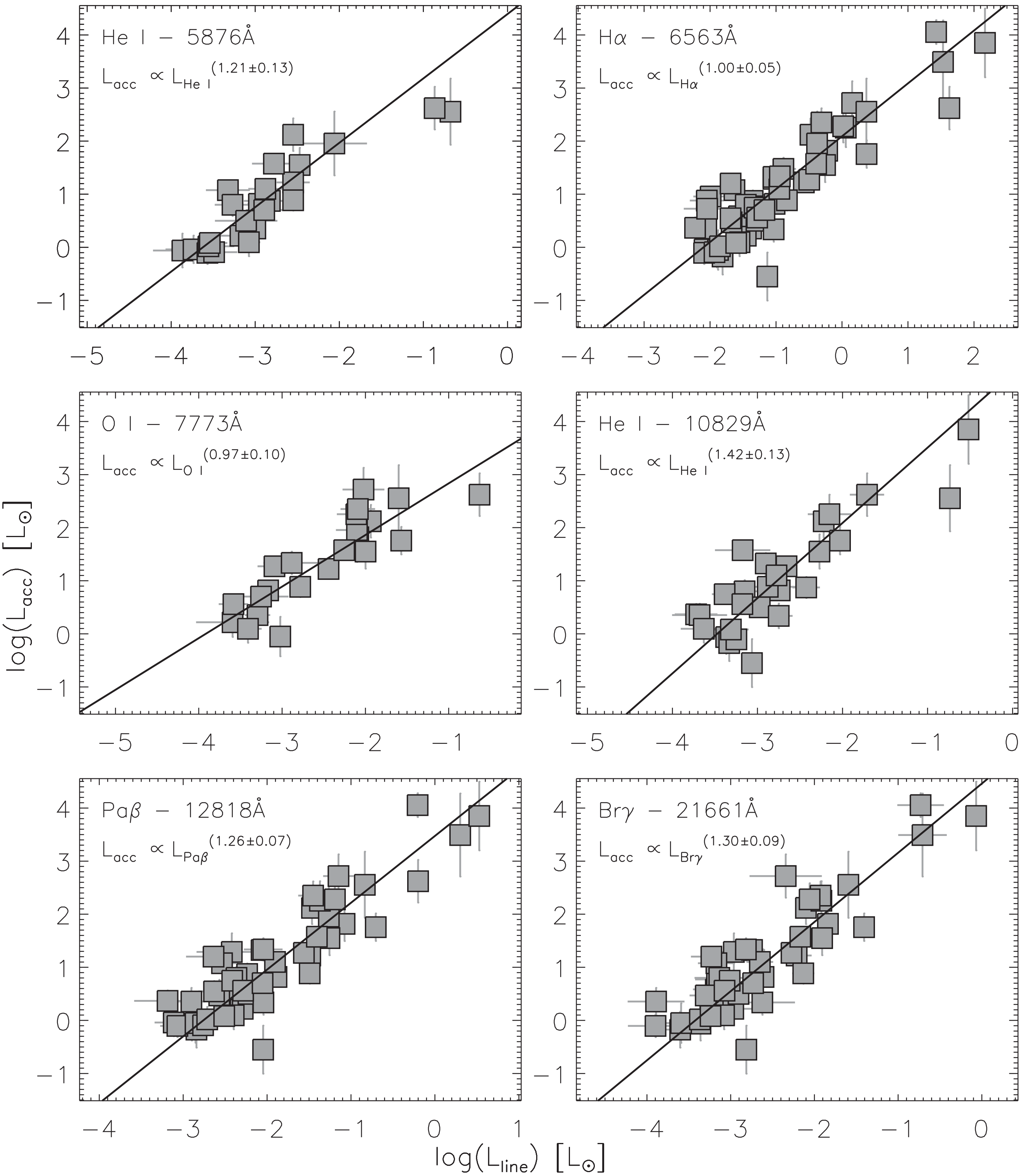

Figure 3. Relationships are displayed between the accretion luminosities determined in Paper I and the line luminosities determined in this work. Each panel shows only the HAeBes where both a clear UV excess and clear emission line detection are made, shown as grey squares; a best-fit to them is shown as a solid-black line (the equation for the line is given below the line descriptor in the top-left of each panel). The relationships are all comparable to each other with the average exponent of each relationship being $\sim 1.19 \pm 0.18$.

Table 2. This table details the number of emission lines detected for each line (Column 4) and the number of these used in determining L_{acc}–L_{line} relationships (Column 5). The number of lines used is less as they must have a corresponding UV excess to be included. The best-fitting slopes and intercepts to the luminosity relationships plotted in Figs 3 and A1 are provided in columns 6 and 7. The best-fitting parameters for the CTTs presented by Alcalá et al. (2014) are provided in the final two columns for comparison.

Line no.	λ (Å)	Line	No. detections	No. used	This work $A \pm \sigma_A$	This work $B \pm \sigma_B$	Alcalá et al. (2014) $A \pm \sigma_A$	Alcalá et al. (2014) $B \pm \sigma_B$
1	3797	H(10-2)	42	30	3.04 ± 0.14	1.14 ± 0.08	2.58 ± 0.27	1.00 ± 0.05
2	3835	H(9-2)	24	16	2.91 ± 0.14	1.06 ± 0.10	2.53 ± 0.27	1.01 ± 0.05
3	3889	H(8-2)	22	18	2.96 ± 0.16	1.17 ± 0.11	2.55 ± 0.29	1.04 ± 0.06
4	4102	Hdelta	23	14	2.65 ± 0.13	1.14 ± 0.10	2.50 ± 0.28	1.06 ± 0.06
5	4340	Hgamma	37	25	2.51 ± 0.10	1.10 ± 0.09	2.50 ± 0.25	1.09 ± 0.05
6	4861	Hbeta	81	51	2.60 ± 0.09	1.24 ± 0.07	2.31 ± 0.23	1.11 ± 0.05
7	5876	He I	31	24	4.39 ± 0.38	1.21 ± 0.13	3.51 ± 0.30	1.13 ± 0.06
8	6300	[O I]	48	28	3.84 ± 0.16	0.94 ± 0.06	– ± –	– ± –
9	6563	Halpha	89	54	2.09 ± 0.06	1.00 ± 0.05	1.50 ± 0.26	1.12 ± 0.07
10	7773	O I	29	21	3.80 ± 0.26	0.97 ± 0.10	3.91 ± 0.51	1.16 ± 0.09
11	8446	O I	57	37	3.61 ± 0.14	0.90 ± 0.05	3.06 ± 0.90	1.06 ± 0.18
12	8498	Ca II	41	29	3.50 ± 0.14	0.91 ± 0.06	2.18 ± 0.38	0.95 ± 0.07
13	8542	Ca II	34	26	3.62 ± 0.15	1.04 ± 0.07	2.13 ± 0.42	0.95 ± 0.08
14	8598	Pa(14-3)	74	49	3.88 ± 0.14	1.13 ± 0.06	– ± –	– ± –
15	8662	Ca II	79	52	3.45 ± 0.12	1.08 ± 0.05	2.20 ± 0.43	0.95 ± 0.09
16	8750	Pa(12-3)	89	55	3.87 ± 0.14	1.34 ± 0.06	– ± –	– ± –
17	8863	Pa(11-3)	78	51	3.81 ± 0.15	1.29 ± 0.07	– ± –	– ± –
18	9015	Pa(10-3)	87	54	3.81 ± 0.15	1.43 ± 0.07	2.99 ± 0.49	1.03 ± 0.09
19	9229	Pa(9-3)	73	46	3.72 ± 0.15	1.31 ± 0.07	3.40 ± 0.47	1.13 ± 0.09
20	9546	Paepsilon	86	54	3.75 ± 0.14	1.38 ± 0.07	3.19 ± 0.58	1.11 ± 0.12
21	10049	Padelta	65	43	4.01 ± 0.17	1.26 ± 0.07	3.33 ± 0.47	1.18 ± 0.10
22	10829	He I	40	27	4.92 ± 0.38	1.42 ± 0.13	2.62 ± 0.57	1.11 ± 0.12
23	10938	Pagamma	71	46	3.76 ± 0.16	1.26 ± 0.07	3.17 ± 0.31	1.18 ± 0.06
24	12818	Pabeta	78	50	3.47 ± 0.13	1.26 ± 0.07	2.45 ± 0.39	1.04 ± 0.08
25	15439	Br(17-4)	27	17	4.25 ± 0.27	0.94 ± 0.11	– ± –	– ± –
26	15556	Br(16-4)	41	26	4.35 ± 0.21	1.05 ± 0.08	– ± –	– ± –
27	15701	Br(15-4)	37	25	4.33 ± 0.21	1.06 ± 0.08	– ± –	– ± –
28	15880	Br(14-4)	33	23	4.27 ± 0.23	1.09 ± 0.09	– ± –	– ± –
29	16109	Br(13-4)	55	40	4.41 ± 0.20	1.21 ± 0.08	– ± –	– ± –
30	16407	Br(12-4)	44	30	4.37 ± 0.22	1.22 ± 0.09	– ± –	– ± –
31	16806	Br(11-4)	61	44	4.60 ± 0.21	1.32 ± 0.08	– ± –	– ± –
32	21661	Brgamma	69	43	4.46 ± 0.23	1.30 ± 0.09	3.60 ± 0.38	1.16 ± 0.07

these hot objects Bertout, Basri & Bouvier (see 1988); Blondel & Djie (see 2006)].[2]

The two categories of emission and accretion can be divided into two outcomes for each case, those with and those without. This gives a total of four possible categories for a star to be in e.g. a star may have a particular line in emission, but no ΔD_B was detected in the star.

Table 3 gives the number of stars split into each category, for each line, and is presented visually in Fig. 4. What the four different categories represent are now detailed.

(i) The first category contains objects for which both emission lines and a UV excess are detected, represented by the green segments in the diagram. This category measures if the line is a good one to one tracer of accretion i.e. excess is present and so is the emission line. Examples of good tracers are Hα, Brγ and Paβ as their emission detections fall predominately in this category.

(ii) The second category indicates how difficult the line is to detect i.e. how insensitive it is. This category is shown in red and contains those stars for which a clear UV excess is detected and for which a mass accretion rate could be derived, but in whose spectra no emission line is detected. An example of this is the oxygen 7773 Å line, for which the majority of ΔD_B detections have no corresponding emission line detection.

(iii) The third category (shown in yellow in the figure) denotes the objects for which an emission line is detected, but no UV excess was detected. Assuming that the emission line is sensitive to accretion, and more readily detectable than an excess, the lines in this category allow the L_{acc} versus L_{line} relationship to be used to infer an accretion luminosity.

(iv) The fourth and final category, shown in orange, contains those objects with no obvious UV excess and no emission in the line of interest. These objects generally have Hα emission, but no sign of other emission lines. If they are actively accreting, the mass accretion rate is well below our detection limits (the lowest log($\dot{M}_{acc}$) detected in Paper I was only −7.78).

The findings in the table and figure highlight that the already established accretion tracing relationships are good ones; Hα, Brγ, and Paβ are all predominately in the green. There are also lines that appear to be poor tracers of accretion. In particular, the Brackett series appears to get worse as an accretion tracer towards the higher order transitions. Such a decline is likely because of the decreasing strength in emission towards the shorter wavelengths; which is supported by the green/red ratio changing between successive orders

[2] Since $\dot{M}_{acc}$ was not determined for these stars, they do not contribute to the fits in Fig. 3.

Table 3. This table details all of the measured emission lines, along with their respective number of detections. The final four columns denote the four categories into which each star of the sample can belong to for a given line; full descriptions are provided in the text. 'Emis' denotes emission line, and ΔD_B denotes the UV excess.

Line number	λ (Å)	Line	Emission lines detected	No. of stars which match the criterion Emis - Y ΔD_B - Y	Emis - N ΔD_B - Y	Emis - Y ΔD_B - N	Emis - N ΔD_B - N
1	3797	H(10-2)	42	36	27	6	22
2	3835	H(9-2)	24	22	41	2	26
3	3889	H(8-2)	22	22	41	0	28
4	4102	Hδ	23	20	43	3	25
5	4340	Hγ	37	31	32	6	22
6	4861	Hβ	81	58	5	23	5
7	5876	He I	31	28	35	3	25
8	6300	[O I]	48	34	29	14	14
9	6563	Hα	89	61	2	28	0
10	7773	O I	29	25	38	4	24
11	8446	O I	57	43	20	14	14
12	8498	Ca II	41	35	28	6	22
13	8542	Ca II	34	32	31	2	26
14	8598	Pa(14-3)	74	56	7	18	10
15	8662	Ca II	79	58	5	21	7
16	8750	Pa(12-3)	89	62	1	27	1
17	8863	Pa(11-3)	78	57	6	21	7
18	9015	Pa(10-3)	87	61	2	26	2
19	9229	Pa(9-3)	73	52	11	21	7
20	9546	Paϵ	86	61	2	25	3
21	10049	Paδ	65	48	15	17	11
22	10829	He I	40	32	31	8	20
23	10938	Paγ	71	52	11	19	9
24	12818	Paβ	78	57	6	21	7
25	15439	Br(17-4)	27	23	40	4	24
26	15556	Br(16-4)	41	32	31	9	19
27	15701	Br(15-4)	37	31	32	6	22
28	15880	Br(14-4)	33	28	35	5	23
29	16109	Br(13-4)	55	46	17	9	19
30	16407	Br(12-4)	44	36	27	8	20
31	16806	Br(11-4)	61	50	13	11	17
32	21661	Brγ	69	50	13	19	9

(with a slight deviation around Br 12-4). The Balmer series demonstrates a similarity to this with the two lowest level transitions, Hα and Hβ, being sensitive to accretion while the remainder are less sensitive. The explanation for this is likely to be the same as for the Brackett series; however, another possible explanation for this could be the UV excess veiling the lines. Veiling of the lines occurs when their intrinsic absorption is filled in by excess emission, which decreases the observed absorption in them and gives them an EW_{obs} closer to 0. However, the brightest of HAeBes makes this scenario unlikely. The Paschen series is an exception to the other two hydrogen series; it maintains a constant level of sensitivity throughout the series. This is due to the location of the lines; the visible region. The SNR here is much higher than the UV and allows us to make a greater number of detections. While in the NIR, due to telluric line correction and IR-excess correction, there is greater margin of error for detection than the visible region. As for the Ca II line, it is likely that the Paschen blending results in more detections for the 8662 line than the other two, as it is blended with the stronger Paschen lines.

For lines leaning more towards being poor tracers of accretion, such as the O I 7773 Å and the He I 5876 Å lines, a possible explanation is that EW_{int} is measured as a sum over the entire line profile. This means that complex profiles, with multiple absorption and emission components, may be missing details of additional contributions to the lines. In extreme cases, stars may be found to have no emission detection despite the clear presence of an inverse P-Cygni profile, where the absorption is strong enough to make the EW_{int} measurement uncertain. Therefore, when considering accretion in HAeBes, analysis of line profiles should be used in combination with line strengths and UV excesses (where possible), to reach a consensus on detection and origin. Such an example is presented by Cauley & Johns-Krull (2014) where their analysis of the lines profiles of the He I 10830 µm line demonstrates strong evidence of MA occurring in HAes, and perhaps from HBes too. Despite the convincing line profiles the detection rate of the line being in overall emission is low, making it a poor tracer in that regard. However, if detected in emission, it can still be used to infer $\dot{M}_{acc}$.

Despite information regarding line profiles being omitted in this work, the L_{acc}– L_{line} relationships hold for the majority of stars and can be used as a diagnostic to infer accretion. Even the lines that have fewer detections correlate well with accretion and can be used if detected.

3.4 Objects without UV excess

One particularly interesting group of stars are those that show lines in emission, but have no detectable UV excess, ΔD_B. This opens up the possibility that the emission lines could be tracing

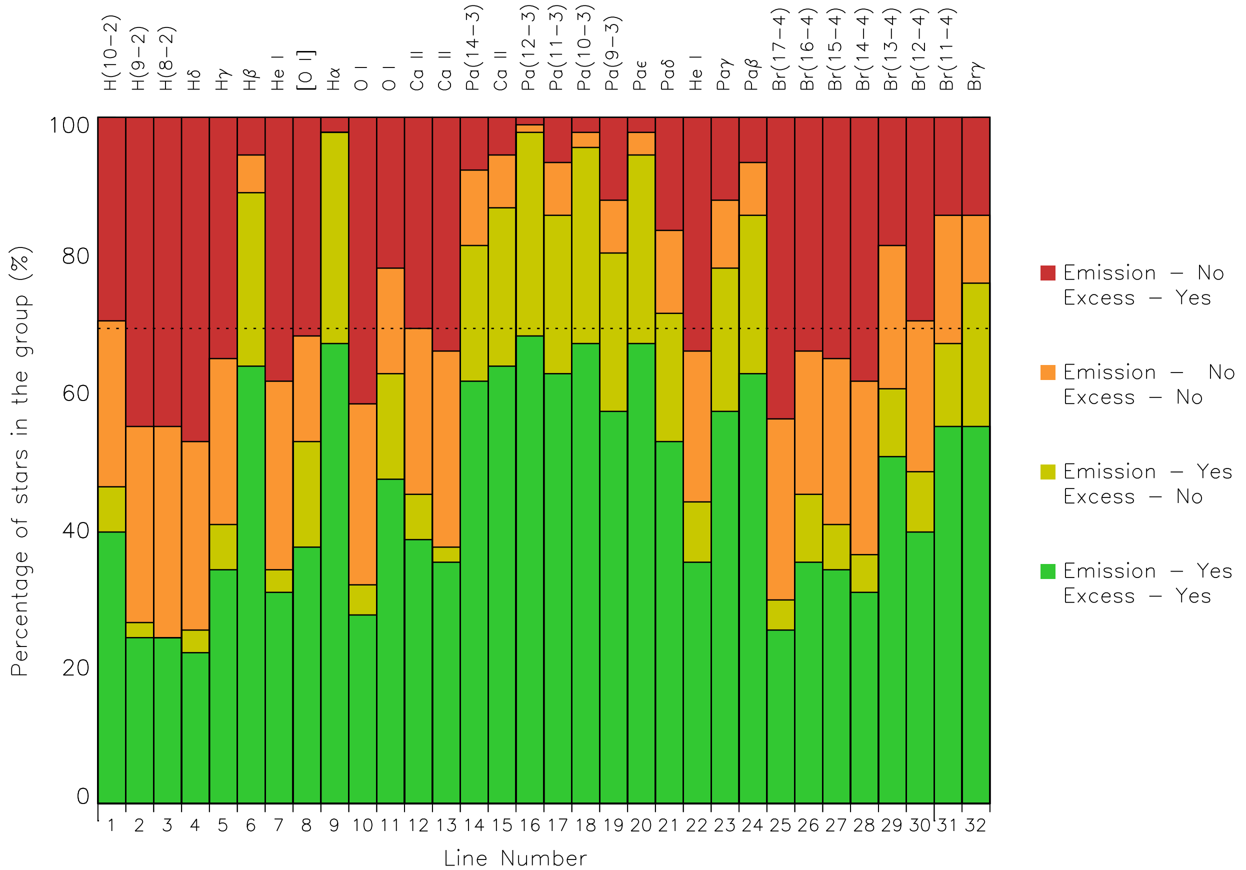

Figure 4. The lines are shown by increasing wavelength along the *x*-axis, with their names given at the top of the plot. Each line is split into four different categories based on whether an emission line was/was not detected, and on whether ΔD_B could/could not be measured. All of the HAeBes examined are represented in this diagram. Details on the meanings of each category are provided in the text. The dashed line denotes the percentage of the sample where a UV excess is detected, 69 per cent, and therefore the closer the green region is to this line the better the tracer. A quick glance demonstrates that Hα, Hβ and the majority of the Paschen series are all sensitive tracers, while both He I lines and weaker Brackett lines are less-sensitive accretion diagnostic lines.

accretion where the accretion rate is below the detection limits of the Balmer excess method. This is now investigated here for the case of Hα.

The line luminosity of Hα is converted into L_{acc}, using the relationship determined previously and tabulated in Table 2. For this test, L_{acc} is calculated for the stars in which only an upper limit could be placed on the Balmer excess (25 stars, see Paper I). The derived L_{acc} is then converted into $\dot{M}_{\mathrm{acc}}$ using the stellar parameters determined in Paper I. This, in turn, is used to predict the resulting ΔD_B values. The predicted excess can be calculated via the ΔD_B versus $\dot{M}_{\mathrm{acc}}$ curves seen in fig. 9 of Paper I.

The predicted ΔD_B agrees with the upper limits measured in Paper I for 21/25 of the objects. This agreement within previous limits for the majority of these stars suggests that the lines in this work are suitable as accretion tracers for inferring $\dot{M}_{\mathrm{acc}}$. For the remaining four objects, a ΔD_B is predicted that is higher than the upper limits previously measured; the values lie just 1σ away from the previous limits. Considering that these four results are only 1σ away, this is not significant to detract from the previous paragraph; the accretion diagnostic properties of the lines still holds in general.

Overall, we can conclude that the ‘yes in emission, no in excess’ criteriòon serves as a positive indicator that a line can be used as an accretion diagnostic line i.e. the line luminosity can be reliably used to infer the accretion rate.

4 CONCLUSIONS

This study provides the largest spectroscopic investigation into accretion rates of HAeBes to date. In addition, the spectral wavelength range covered in these stars is much larger than any other HAeBe investigation, which allows an investigation from the UV up to the NIR at 2.5 µm. The combination of a large sample, 91 objects, and huge wavelength coverage allows for the most robust statistical investigation into the emission lines in HAeBes to be performed to date.

Line luminosities were obtained for 32 different lines. The line luminosities are observed to be correlated with the accretion luminosities – by implication they are therefore correlated to the mass accretion rates. We focused on expanding our understanding of relationships between L_{acc} and L_{line} in HAeBes, and how these relate to similar relationships observed in CTTs. The large size of the sample and large spectral coverage resulted in a 10-fold increase in accretion line diagnostics for HAeBe stars compared to what was known in the literature.

The following key points are found.

(i) Relationships are obtained between L_{acc} and L_{line} for 32 different emission lines. In all cases a best fit is made to these lines, with the average correlation being $L_{\mathrm{acc}} \propto L_{\mathrm{line}}^{1.16\pm0.15}$. The fact that both UV excess and emission lines were measured simultaneously makes these the most robust set hitherto published.

(ii) We find that all lines can be used as an accretion tracer. Additionally, it was shown by extrapolation, for the case of Hα, that an emission line could be used to infer low-mass accretion rates that cannot normally be measured by a UV excess. This is particularly applicable for the hotter objects where their large intrinsic UV output makes the detection of weak UV excess emission difficult.

(iii) The relationship $L_{\rm acc} \propto L_{\rm line}^{1.16\pm0.15}$ obtained for the HAeBes in this work agrees with the relationship observed in CTTs by Alcalá et al. (2014), where $L_{\rm acc} \propto L_{\rm line}^{1.08\pm0.08}$; the relationship is steeper for the HAeBes. On an individual line basis, some variations are seen in the relationship between the two. Notably the Ca and He lines display complex line profiles that behave differently for both types of sources; this warrants further investigation.

(iv) An assessment of the sensitivity of each line as an accretion tracer has been performed through a comparison of respective emission line and UV-excess detection rates. We confirm that the well-known accretion tracers for CTTs, such as Hβ, Hα, Paβ and Brγ, are also tracers of accretion in HAeBe stars.

(v) The sheer number of objects and emission lines analysed here provide robust relationships between $L_{\rm acc}$ and $L_{\rm line}$ for an exceptional wavelength coverage. In particular, known accretion tracing lines have been further verified and new observational windows have been opened up for measuring $\dot{M}_{\rm acc}$ in HAeBes e.g. Hβ in the blue *B*-band region, Paβ in the *J*-band region and Br(13-4) in the *H*-band region. In the visible region, the Paschen series shows consistent sensitivity between lines. These new diagnostics will prove valuable in future observations.

(vi) Additionally, some lines can be considered poor tracers of accretion due to a low rate incidence of detection of emission lines e.g. $[\mathrm{O\,I}]_{\lambda 6300}$ and He I 5876 Å. However, when these lines are detected in emission they are nearly always associated with a UV excess i.e. associated with accretion, and the relationship holds. Since this aspect is present for all lines and relationships tested here, it is likely there is a deeper physical connection. For example, in the case of $[\mathrm{O\,I}]_{\lambda 6300}$ it is suspected that photospheric UV photodissociates OH in upper layers of the disc, giving rise to this emission (Acke, van den Ancker & Dullemond 2005).

(vii) The high number of correlations is a topic that has been discussed recently by Mendigutía et al. (2015), where the authors found that the relationships observed between $L_{\rm acc}$ and $L_{\rm line}$ appear to be a consequence of them being directly related to the star's own stellar luminosity (see also Boehm & Catala 1995). Therefore, the line luminosities may not physically arise due to accretion on to the star, but they can still serve as a diagnostic for obtaining accretion rates.

In order to gain knowledge on the physical origin of the emission lines, and their association with accretion, the line profiles themselves must be considered. Work on line profiles so far has demonstrated notable differences between CTTs and HAeBes so far (Hamann & Persson 1992a,b; Cauley & Johns-Krull 2014, 2015). Connecting these changes with both the relationships determined here, the underlying mathematical relationships (Mendigutía et al. 2015) and the large number of lines obtained with X-Shooter is the next challenge; this will be presented in a future paper by the authors.

ACKNOWLEDGEMENTS

JRF gratefully acknowledges a studentship from the Science and Technology Facilities Council of the UK. JDI gratefully acknowledges support from the DISCSIM project, grant agreement 341137, funded by the European Research Council under ERC-2013-ADG. This work has made use of NASA's Astrophysics Data System; it has also made use of the SIMBAD data base, operated at CDS, Strasbourg, France. The authors would like to extend their thanks to the anonymous referee who helped strengthen the manuscript.

REFERENCES

Acke B., van den Ancker M. E., Dullemond C. P., 2005, A&A, 436, 209
Alcalá J. M. et al., 2014, A&A, 561, A2
Bertout C., 1989, ARA&A, 27, 351
Bertout C., Basri G., Bouvier J., 1988, ApJ, 330, 350
Blondel P. F. C., Djie H. R. E. T. A., 2006, A&A, 456, 1045
Boehm T., Catala C., 1995, A&A, 301, 155
Calvet N., Gullbring E., 1998, ApJ, 509, 802
Calvet N., Muzerolle J., Briceño C., Hernández J., Hartmann L., Saucedo J. L., Gordon K. D., 2004, ApJ, 128, 1294
Castelli F., Kurucz R. L., 2004, preprint (arXiv:astro-ph/0405087)
Cauley P. W., Johns-Krull C. M., 2014, ApJ, 797, 112
Cauley P. W., Johns-Krull C. M., 2015, ApJ, 810, 5
Cutri R. M. et al., 2003, The IRSA 2MASS All-Sky Point Source Catalog, NASA/IPAC Infrared Science Archive. Available at: http://irsa.ipac.caltech.edu/applications/Gator/
Dahm S. E., 2008, ApJ, 136, 521
Donehew B., Brittain S., 2011, ApJ, 141, 46
Eiroa C. et al., 2001, A&A, 365, 110
Eiroa C. et al., 2002, A&A, 384, 1038
Fairlamb J. R., Oudmaijer R. D., Mendigutía I., Ilee J. D., van den Ancker M. E., 2015, MNRAS, 453, 976 (Paper I)
Finkenzeller U., Mundt R., 1984, A&AS, 55, 109
Garrison, L. M., Jr, 1978, ApJ, 224, 535
Ghosh P., Lamb F. K., 1979, ApJ, 232, 259
Gullbring E., Hartmann L., Briceno C., Calvet N., 1998, ApJ, 492, 323
Gullbring E., Calvet N., Muzerolle J., Hartmann L., 2000, ApJ, 544, 927
Hamann F., Persson S. E., 1992a, ApJS, 82, 247
Hamann F., Persson S. E., 1992b, ApJS, 82, 285
Herbig G. H., 1960, ApJS, 4, 337
Herczeg G. J., Hillenbrand L. A., 2008, ApJ, 681, 594
Ilee J. D., Fairlamb J., Oudmaijer R. D., Mendigutía I., van den Ancker M. E., Kraus S., Wheelwright H. E., 2014, MNRAS, 445, 3723
Ingleby L. et al., 2013, ApJ, 767, 112
Kausch W. et al., 2015, A&A, 576, A78
Koenigl A., 1991, ApJ, 370, L39
Kurucz R. L., 1993, SYNTHE Spectrum Synthesis Programs and Line Data. Smithsonian Astrophysical Observatory, Cambridge
Meeus G., Waters L. B. F. M., Bouwman J., van den Ancker M. E., Waelkens C., Malfait K., 2001, A&A, 365, 476
Mendigutía I., Calvet N., Montesinos B., Mora A., Muzerolle J., Eiroa C., Oudmaijer R. D., Merín B., 2011, A&A, 535, A99
Mendigutía I. et al., 2013, ApJ, 776, 44
Mendigutía I., Oudmaijer R. D., Rigliaco E., Fairlamb J. R., Calvet N., Muzerolle J., Cunningham N., Lumsden S. L., 2015, MNRAS, 452, 2837
Modigliani A. et al., 2010, Proc. SPIE, 7737, 773728
Mottram J. C. et al., 2011, A&A, 525, A149
Munari U., Sordo R., Castelli F., Zwitter T., 2005, A&A, 442, 1127
Muzerolle J., Hartmann L., Calvet N., 1998, ApJ, 116, 455
Muzerolle J., D'Alessio P., Calvet N., Hartmann L., 2004, ApJ, 617, 406
Rigliaco E., Natta A., Testi L., Randich S., Alcalà J. M., Covino E., Stelzer B., 2012, A&A, 548, A56

Shu F., Najita J., Ostriker E., Wilkin F., Ruden S., Lizano S., 1994, ApJ, 429, 781
Skrutskie M. F. et al., 2006, ApJ, 131, 1163
Smette A. et al., 2015, A&A, 576, A77
Thé P. S., de Winter D., Perez M. R., 1994, A&AS, 104, 315
Uchida Y., Shibata K., 1985, PASJ, 37, 515
van den Ancker M. E., Bouwman J., Wesselius P. R., Waters L. B. F. M., Dougherty S. M., van Dishoeck E. F., 2000, A&A, 357, 325
Vernet J. et al., 2011, A&A, 536, A105
Vieira S. L. A., Corradi W. J. B., Alencar S. H. P., Mendes L. T. S., Torres C. A. O., Quast G. R., Guimarães M. M., da Silva L., 2003, ApJ, 126, 2971
Vink J. S., Drew J. E., Harries T. J., Oudmaijer R. D., 2002, MNRAS, 337, 356
Vink J. S., Drew J. E., Harries T. J., Oudmaijer R. D., Unruh Y., 2005, MNRAS, 359, 1049

SUPPORTING INFORMATION

Additional Supporting Information may be found in the online version of this article:

Table 1. This table provides the EW measurements for the Hα line in all objects.
(http://www.mnras.oxfordjournals.org/lookup/suppl/doi:10.1093/mnras/stw2643/-/DC1).

APPENDIX A: ADDITIONAL LUMINOSITY RELATIONSHIPS

The sheer number of lines analysed here warrants the use of an appendix for easy reading. In here, Fig. A1 displays the accretion luminosity versus line luminosity relationships for all 32 lines analysed (an extension of Fig. 3). The best fits to the data are present in the figure. Where possible, the data on CTTs from Alcalá et al. (2014) are also included for comparison.

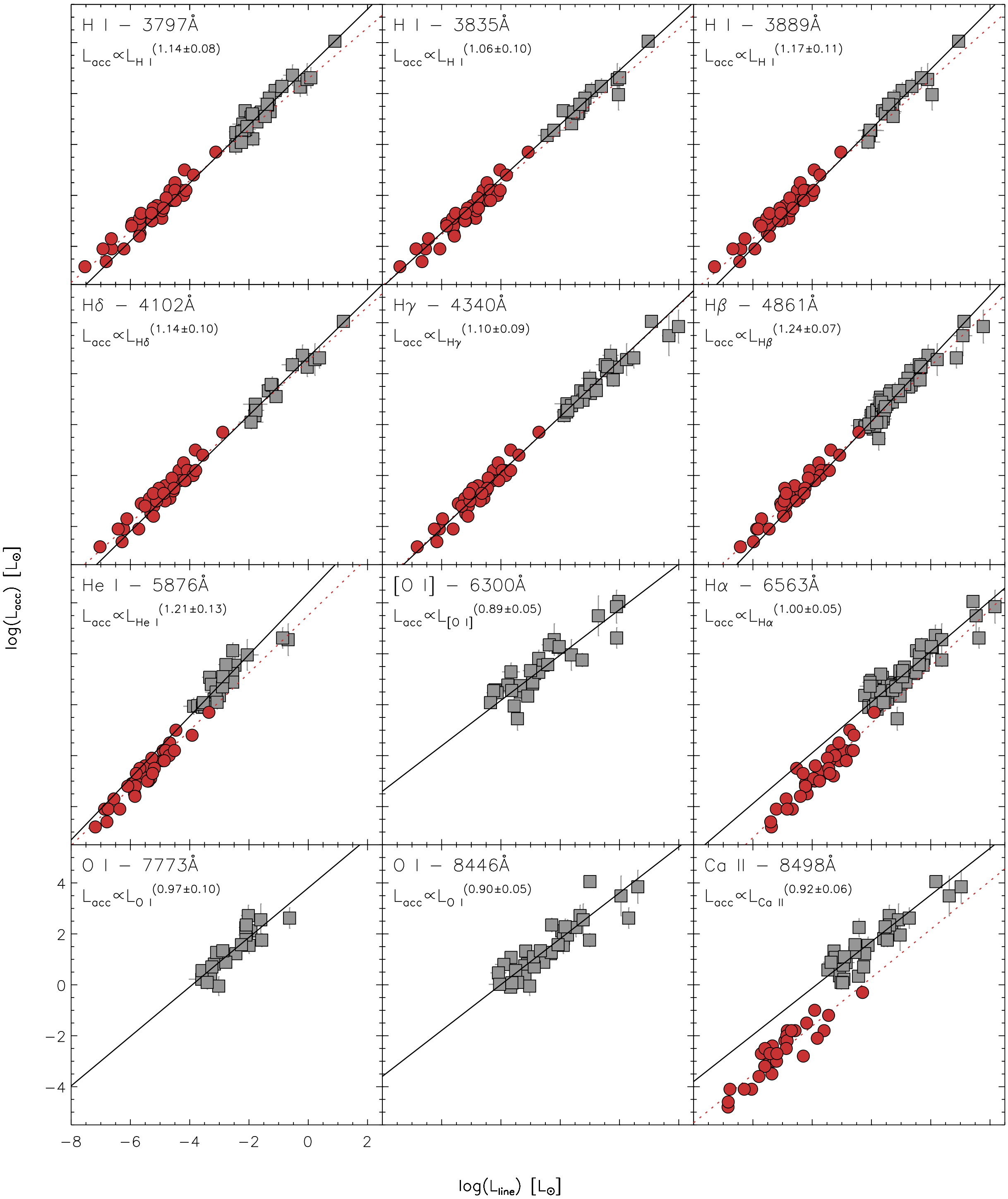

Figure A1. The accretion luminosity, as calculated directly from the UV excess, against the line luminosities. Each panel shows only the HAeBes where both a clear UV excess and clear emission line detection are made, shown as grey squares; a best fit to them is shown as a solid-black line (the equation for the line is given below the line descriptor in the top-left of each panel, and is also given in 2). Where applicable, the data on CTTs from Alcalá et al. (2014) are plotted for comparison, as red circles, along with their best fit as a dashed-red line.

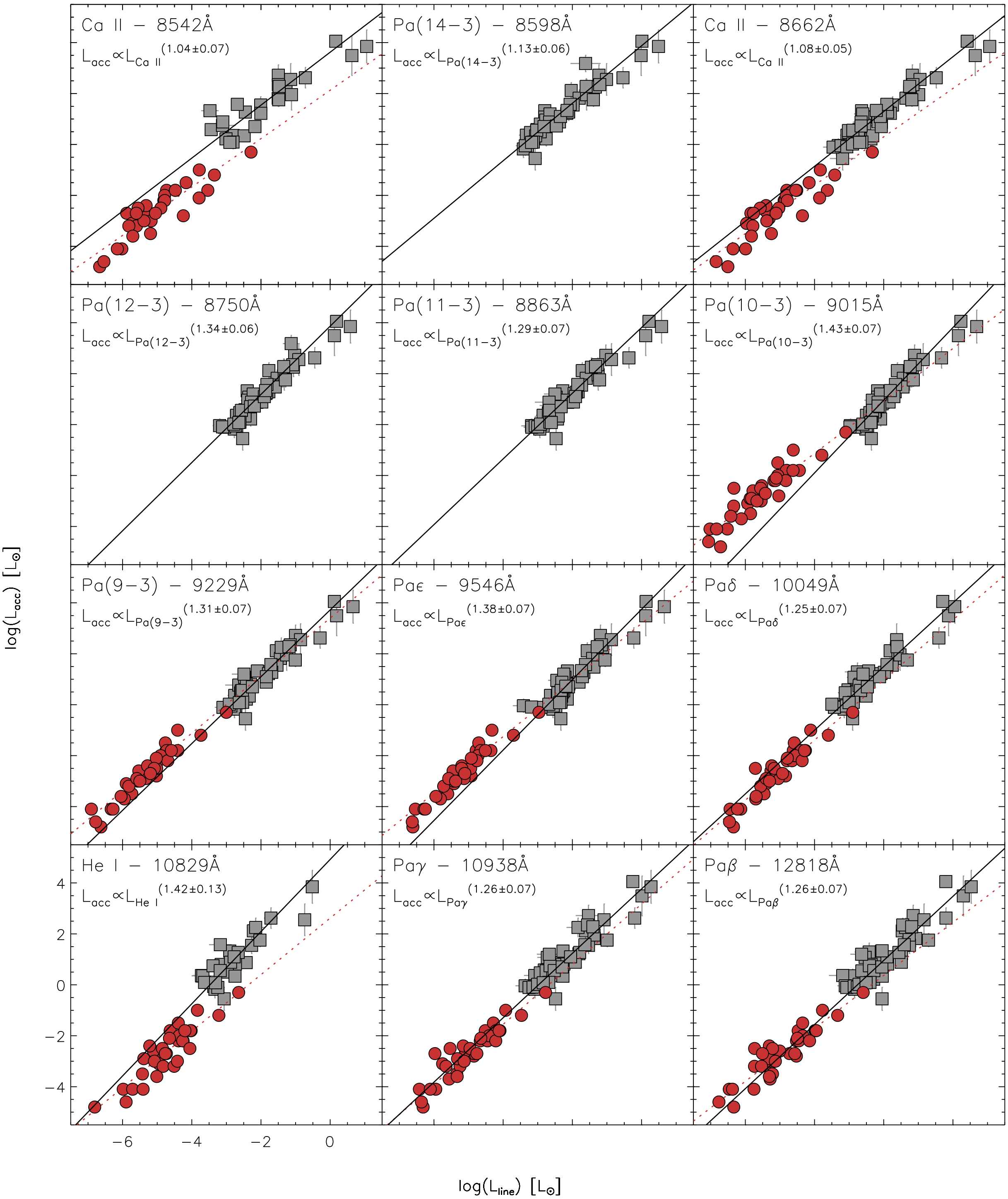

Figure A1 – *continued*

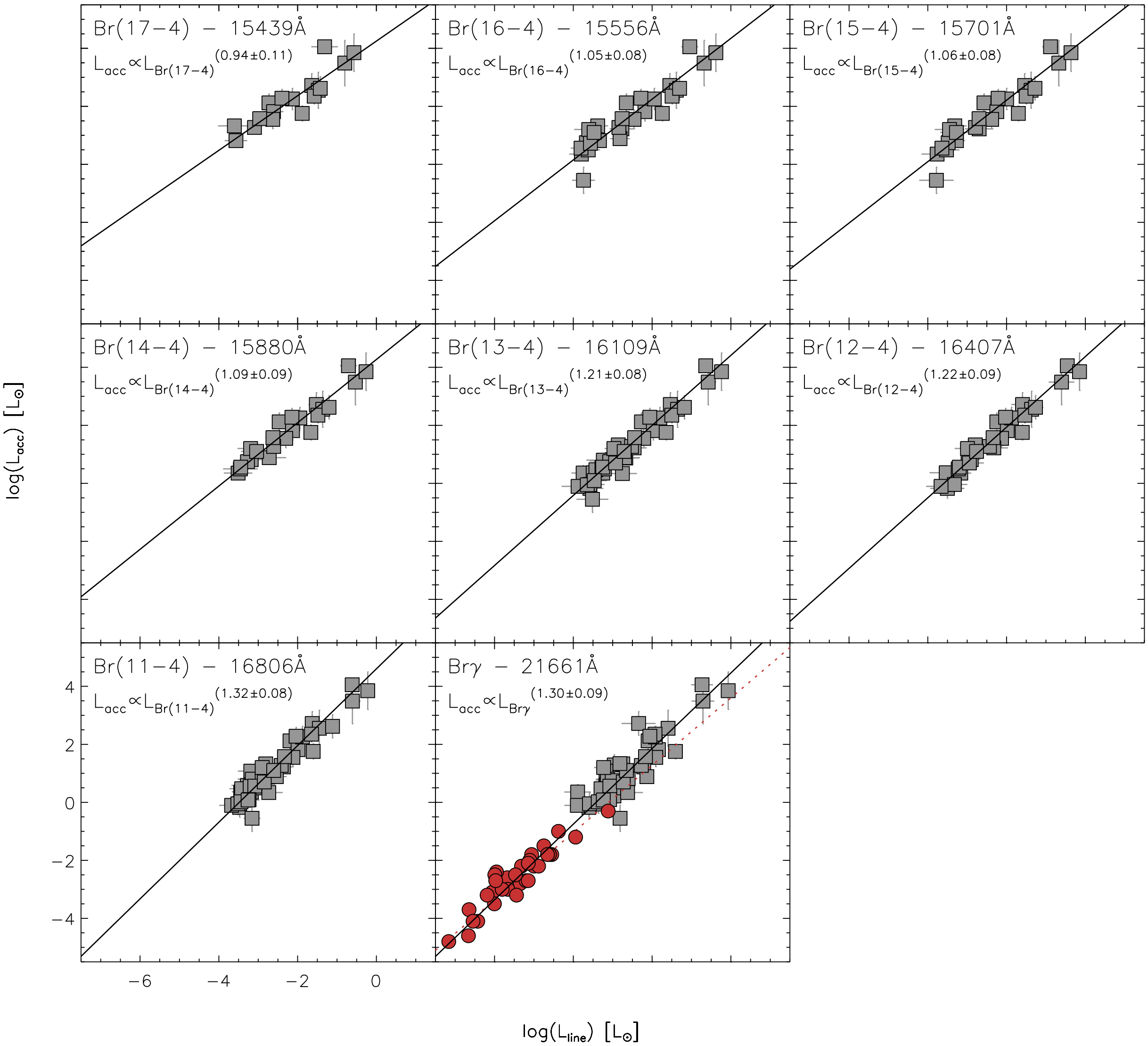

Figure A1 – *continued*

This paper has been typeset from a TEX/LATEX file prepared by the author.